Original Article

Institution of MECHANICAL ENGINEERS
Journal of AEROSPACE ENGINEERING

Proc IMechE Part G:
J Aerospace Engineering
2017, Vol. 231(2) 319–325

DOI: 10.1177/0954410016636911
uk.sagepub.com/jaero
SAGE

Numerical simulation of fairing separation test for hypersonic air breathing vehicle

Ankit Raj, K Anandhanarayanan, R Krishnamurthy and Debasis Chakraborty

Abstract

Fairings are provided to cover hypersonic air breathing vehicle to protect it from adverse aerodynamic loading and kinetic heating. Separation dynamics of fairings is an important event in the launch of vehicle. Extensive computational fluid dynamics simulations are carried out for the design of fairings and vehicle and selection of time sequences of various separation events. A ground test of fairing separation is conducted in the sled facility to check the structural integrity and functionality of various separation mechanisms and flight hardware. Simulations have been carried out to study the separation dynamics of fairings at test conditions using grid-free Euler solver to get the aerodynamic loads and the loads are integrated to get the trajectory of fairings. The aerodynamic loads are provided to verify the structural integrity of various components and the trajectory of panels is used in the test planning. The pressure distributions on the vehicle are compared with the test results.

Keywords

Fairing separation, grid-free method, computational fliud dynamics, rigid body dynamics, aerodynamic damping

Date received: 24 February 2015; accepted: 7 January 2016

Introduction

The quest for efficient hypersonic air breathing propulsion led to the development of scramjet engine from early 1960s.[1] A typical cruise hypersonic air-breathing mission is explained in Pannerselvam et al.[2] which aims at demonstrating autonomous functioning of airframe integrated scramjet engine for 20 s at Mach number 6 and 30 km altitude. Ground launch option is considered for the proposed mission and the vehicle is housed above a launch vehicle (LV) booster to be carried to the desired altitude. To protect the cruise vehicle (CV) from the adverse aerodynamic heating in the ascend phase, it is covered with two sets of fairings viz., nose panels and cylindrical panels as shown in Figure 1 which need to be jettisoned. The nose panels separate in yaw plane and the cylindrical panels separate in pitch plane of the vehicle. The safe separation of the fairings must be ensured for the success of the mission. The nose panels are initially opened to a small angle with help of pyro force and further opened to a pre decided opening angle with help of aerodynamic forces and then, released from the vehicle. After nose panel reaching to a safe distance, the opening of cylindrical panels is initiated. After the cylindrical panels open to a pre-set release angle with aid of aerodynamic forces, it is released. The fairings are attached to the LV through cylindrical hinges and the hinges are designed such that the fairings are released at the pre-set release angle. Further, the fairings are separated with the help of aerodynamic forces to a safe distance and then, the vehicle is injected to the atmosphere. The safe separation of the fairings is one of the important events in the mission. Fairing separation in the atmosphere is extensively studied by various other researchers. Dagan and Arad[3] have simulated the shroud separation of a high velocity missile using off-line generated aerodynamic loads using experiment and computational fliud dynamics (CFD) data base. Cavallo and Dash[4] have simulated the shroud separation using adaptive unstructured grid method. Chamberlain[5] has used finite element method for transient compressible flows in the simulation and analysis of high endoatmospheric defence interceptor (HEDI) shroud separation. Experimental facilities[6] have been established to carry out such separation studies. Earlier, we

Defence Research and Development Laboratory, Hyderabad, India

Corresponding author:
Debasis Chakraborty, Defence Research and Development Laboratory, Kanchanbagh, Hyderabad 500058, India.
Email: debasis_cfd@drdl.drdo.in

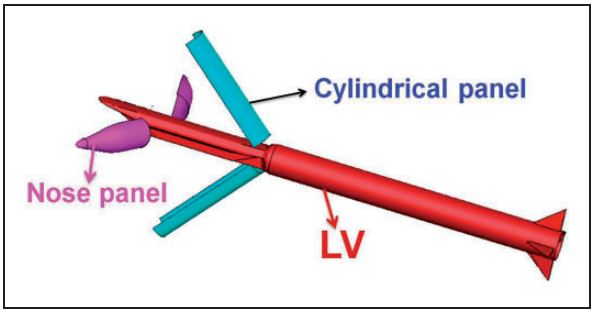

Figure 1. Heat shield separation system for hypersonic vehicle.

have carried out the separation dynamics of fairing at hypersonic Mach number using a grid-free solver[7] and the separation sequences and optimum releasing angles are determined for the safe separation of fairings. The aerodynamic forces and moments on fairings and vehicle are provided for the structural design of these components and other mechanical devices.

Many mechanisms including fairing hinges need to be tested on ground for their functionality at flow conditions that simulate the flight dynamic pressure, aerodynamic forces and moments. Rocket sled facilities are generally well established in many countries for high speed applications.[8–10] In this facility, the vehicle (sled) which carries the test object is accelerated to desired Mach number along the rails by rocket motors, guided by slippers which wraps around the rail to provide stability and restraint. The cylindrical panel separation studies are carried out on ground using rocket sled facility to simulate dynamics of fairing separation. Actual flight hardware designed for hypersonic Mach number 6 at 30 km altitude is used in the ground test. The loads would be 84 times that of flight loads if the test to be conducted at same Mach number in the ground. Therefore, the Mach number has to be chosen such that the dynamic pressure for the flight condition needs to be simulated in the ground and that can be established between Mach numbers 0.6 and 0.7. The test article is mounted on a rail rocket sled as shown in Figure 2 such that the panels open azimuthally in the ground test to avoid interference with the sled and the sled is accelerated to the test Mach number and the separation studies are conducted. The test plan requires approximate trajectory of panels to position the high speed cameras to capture the trajectories of panels and also to ensure the safety of humans around and neighbouring facilities. In the present paper, CFD simulations of cylindrical panel separation dynamics at ground test conditions are presented. An integrated CFD-six degrees of freedom (6-DOF) code[11] is applied to obtain the trajectory of panels for planning of the test and aerodynamic loads for designing of attachments to the sled. Quasi steady simulations, i.e. the steady state CFD simulations, are carried out at each panel position to obtain the aerodynamic forces and

Figure 2. Vehicle on the sled.

moments and they are integrated to obtain new position of panels. The aerodynamic damping is modelled using transpiration boundary condition. The developed aerodynamic damping model is validated for isolated missiles and store separation from wing. The details of the aerodynamic damping model and the validation results are available in Anandhanarayanan.[11] The effect of aerodynamic damping on the panel separation is also studied for the present case.

Methodology

The simulation is commenced from initiation of cylindrical panel opening. It is assumed that the sled has reached to its test Mach number at this instant. The grid-free solver is applied to get the aerodynamic forces on panels and vehicle. During opening of panels, 1-DOF for opening angle is solved for each panel using their respective hinge moments. The rotational motion of panels are represented by, neglecting frictional and damping forces,

$$\widetilde{I_{yy}}\,\ddot{\theta} = M_{HM} \tag{1}$$

where $\widetilde{I_{yy}}$ is moment of inertia of panel about hinge axis, θ is the opening angle and M_{HM} is the aerodynamic moment about hinge. The double dot represents second derivative with respect to time. The above equation is integrated to obtain opening angle and angular rate of panels. The linear motion of the vehicle along the rail is solved by integrating linear acceleration due to axial force of the vehicle and the un-separated panels using the following expression:

$$M\,\ddot{x} = F_A \tag{2}$$

where M is the total mass of vehicle and un-separated panels, F_A is the total force along the longitudinal axis of the vehicle and x is the linear displacement. As the panels reach to their respective release angle, the panels are detached from the vehicle and 6-DOF equations of motion are solved for those panels.

In the flight condition, aerodynamic loads on panels are not symmetric and the gravity force aids in opening of bottom panel (BP), whereas, it opposes the opening of top panel (TP). Therefore, the release angles for top and BPs are different. In the ground test, the vehicle is placed such that the panels open azimuthally, therefore, the gravity force acts symmetrically but the aerodynamic forces are different due to asymmetry of vehicle. Since the release angle is designed for the flight condition, there may be a delay in separation of one panel in the test. During this period, forces on the un-separated panels are added to the vehicle for the dynamic simulation. After release of panels, the equations of motion for three angular and three linear components are solved with a 6-DOF solver to obtain positions of the panel. Pre-processor is applied to generate connectivity for this position and then, the grid-free Euler solver is applied to get the aerodynamic loads on panels and vehicle. The above procedure is repeated till the panels "fall on the ground".

Details of geometry and point distribution

The geometry consists of a CV, two cylindrical panels and a portion of the LV which is shown schematically in Figure 1. The panels are attached to the LV with the help of hinges. The cylindrical panels are opened with help of aerodynamic forces to the pre-decided angles and then detached from the vehicle. The grid-free Euler solver[12] is used to obtain the aerodynamic loads on panels and vehicle. The grid-free solver requires a cloud of points in the domain on which the governing partial differential equations are solved and a set of neighbours around each point to discretize the spatial derivatives using the least squares method. The cloud of points can be generated adapting different procedures like structured, unstructured, Cartesian, hybrid grids or other methods such as space filling with objects/ points and thus obtained distribution points should be able to resolve the flow features. Further details of cloud generation methodologies are explained in Anandhanarayanan[11] and Deshpande et al.[12] One of the methods of generation such cloud would be generating grids around different components and considering only the points from different component grids.[13] This method is known as chimera cloud method and is similar to chimera grid method, except there is no interpolation involved in this method and there is no constraint on mesh spacing in the overlapped regions. It is easy to implement convergence acceleration methods and code parallelization in multi-core systems.

In the present work, unstructured grids around CV and cylindrical panels are generated separately and are overlapped to get the distribution of points around full configuration. The points that lie inside the body, known as solid points, are removed using efficient blanking algorithm. Figure 3 shows chimera cloud of points before and after blanking of the solid points. A large computational domain consists of inflow boundary at 15 m upstream, far-field boundaries at ± 30 m and outflow boundary at 35 m aft of the CV. Full tetra mesh is generated around the CV configuration with proper clustering of points where the flow gradients are expected to be high. The computational domain consists of 2.2 million nodes. The grid generation is one time effort and the points around panels are moved with respect to CV during dynamic simulation based on 6-DOF output, the connectivity is regenerated for that position and solver is applied on the data structure.

Computational tools

A store separation dynamics (SSD) suite[11] which consist of a pre-processor, a grid free Euler flow solver using entropy variable (q) based least square kinetic upwind method (q-LSKUM) and a 6-DOF trajectory solver is used to simulate the cylindrical panel separation dynamics. The grid-free solver requires a cloud of points within computational domain and a set of neighbours (connectivity) around each point. The pre-

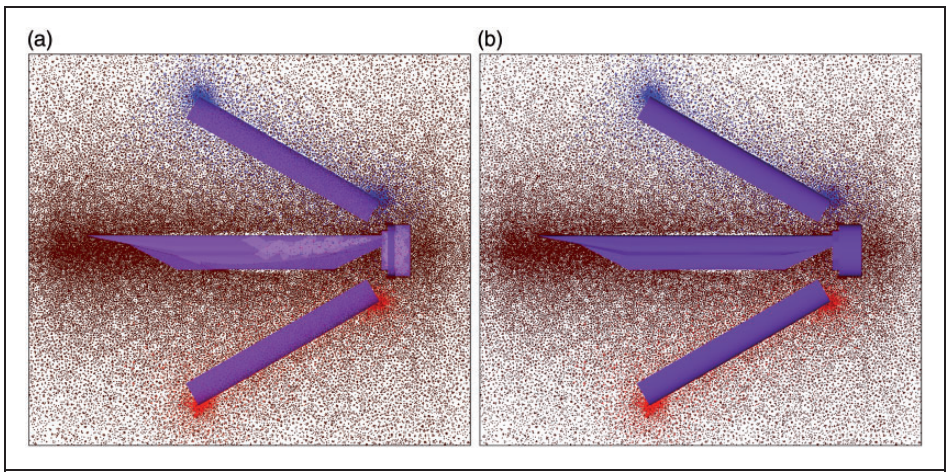

Figure 3. Chimera cloud of point. (a) Before blanking. (b) After blanking.

processor generates the data structure using the overlapped clouds of points around the CV and cylindrical panels as mentioned earlier. The points of one cloud that lie inside other component (solid points) are blanked using the surface normal test. The connectivity for each point is obtained using nodal connectivity from the background grid and in the overlapping region, the connectivity is enhanced from other clouds using efficient search algorithms.

The grid-free CFD solver was developed using least squares kinetic upwind method (LSKUM).[14] LSKUM stems from kinetic flux vector splitting (KFVS) method in which the Boltzmann equation is split based on sign of molecular velocity and taking ψ-moments lead to Courant Isaacs and Rees (CIR) split Euler equations in the continuum space. In LSKUM, the differential form of Euler equations is solved. The spatial derivatives of fluxes are discretized using least squares method. The connectivity is split in three coordinate directions and the split connectivity is used in discretizing the split flux derivatives. A defect correction technique on the entropy variable (q)[15] is employed to achieve higher order accuracy in space. Kinetic characteristic boundary conditions (KCBC) are used to treat boundary conditions. The solver is parallelized using message passing interface (MPI) and lower-upper symmetric Gauss Seidel is implemented in LSKUM frame work for convergence acceleration. In the present study, the fairing separation studies are carried out using quasi-steady approach. In this approach, the solution is allowed to reach steady state, then the fairings are moved to new position. Therefore, relative speed between vehicle and fairings is not simulated. Therefore, instead of zero normal velocity (slip wall boundary conditions, $\vec{v} \cdot \vec{n} = 0$) as wall boundary condition, the local surface normal velocity of fairing (surface transpiration boundary condition, $\vec{v} \cdot \vec{n} = (\vec{v_b} + \vec{\omega} \times \vec{r}) \cdot \vec{n}$)[16,11] is imposed at each wall boundary points. The linear velocity $\vec{v_b}$ and angular rate $\vec{\omega}$ of fairing obtained from the 6-DOF solver is used to impose the above boundary condition. This boundary condition simulates the relative velocity of fairing and as well models the aerodynamic damping due to linear and angular velocity of fairings.

The trajectory of panels is simulated using an integrated 6-DOF solver. In the present study, the inertial frame is attached to the vehicle and body frames are attached to each panel. The translational motion of panels in the body frame is given as,

$$m\left(\dot{\vec{v_b}} + \vec{\omega} \times \vec{v_b}\right) = \vec{F_b} \tag{3}$$

where m is the mass of panel, $\vec{v_b}$ is the linear velocity of the panel in the body frame, $\vec{\omega}$ is the angular velocity and $\vec{F_b}$ is the force acting on the panel. The rotational motion of the panels is given by,

$$I\dot{\vec{\omega}} + \vec{\omega} \times I\vec{\omega} = \vec{M_b} \tag{4}$$

where I is the moment of inertia tensor of panel about their centre of gravity (cg), and $\vec{M_b}$ is the moment about cg of the panel. The above equations are solved using fourth-order Runge-Kutta method. The aerodynamic forces and moments are obtained from the solver in the inertial frame and they are transformed to body frame for solving the above equations of motion. The velocity and displacements are solved in the body frame and they are transformed to inertial frame to position the panels with respect to CV and for imposing transpiration velocity boundary condition in the solver. Quaternion representation is used for transforming vectors. The relative displacement and angles are provided to the pre-processor to position the panels relative to the CV and generating data structure. The above codes are integrated to form SSD suite and is applied to separation studies of air to air missiles from fighter aircraft.[17]

Results and discussions

For grid dependence study, the BP and TP are positioned at lateral displacements of 1.65 and 1.5 m from

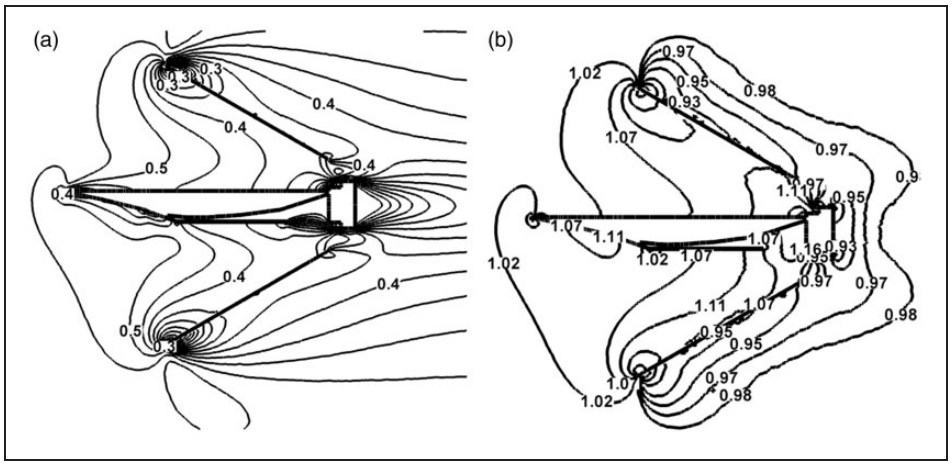

Figure 4. Mach and pressure contours in pitch plane. (a) Mach contours. (b) Pressure contours.

the centre line with opening angles of 50° and 40°, respectively. Figure 4 shows Mach contours and pressure contours in the pitch plane at Mach 0.6. There is strong compression near nose tip of vehicle and panel tips and further expansion behind the panels. Table 1 presents the comparison of axial force (CA) , side force (CS) and hinge moment (cn) coefficients of BP and TP at Mach 0.6 on two different grid sizes of 0.74 and 2.2 million points. A close match of the data (<2%) demonstrates the results are grid independent.

Table 1. Aerodynamic coefficients on two different grids coarse (0.74 M) and fine (2.2 M).

Component	Grid	CA	CS	Cn
BP	Coarse	3.837	3.095	−5.150
	Fine	3.938	3.178	−5.282
TP	Coarse	2.794	−3.243	3.408
	Fine	2.827	−3.282	3.445

Figure 5 shows the time history of lateral displacement and yaw angular rate at Mach 0.7 with and without aerodynamic damping. Without aerodynamic damping, the panels continuously traverse away from CV, the yaw rate oscillates between 500° and 1000° per second and the panel rotates undamped about the centre of gravity. Whereas, with aerodynamic damping, the panels initially traverse away from the CV, later it comes back towards the CV and fall behind the CV. Although, initially, the yaw rates of the both the panels are similar to the undamped case; but the rates are in reverse direction in the later part. As the yaw angle crosses 90°, the panel introduces inward force which makes the panel move towards the CV. Similar behaviour is observed for roll angle, pitch angle and vertical displacements (Figure 6) for Mach number 0.6 and 0.7 with aerodynamic damping. The values

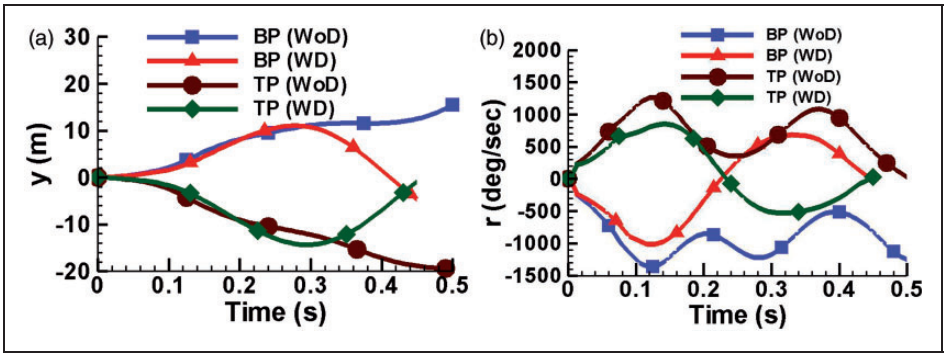

Figure 5. Time history of (a) lateral displacement (m) and (b) yaw rate (°/s) for $M = 0.7$ with and without aerodynamic damping.

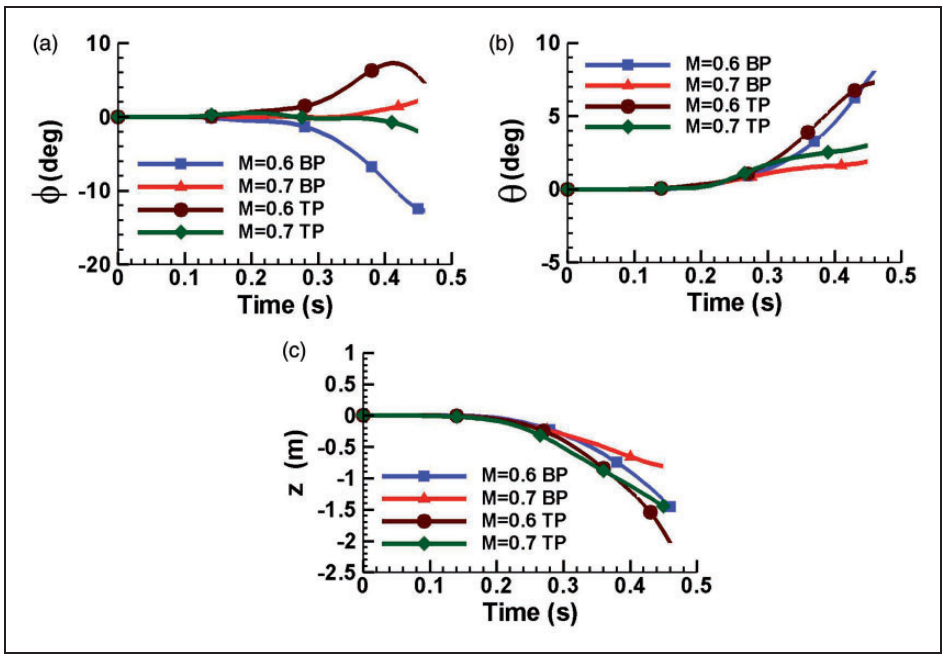

Figure 6. Time history comparison of (a) roll angle (deg) (b) pitch angle (deg) and (c) vertical displacement (m) for Mach 0.6 and 0.7 for BP and TPs.

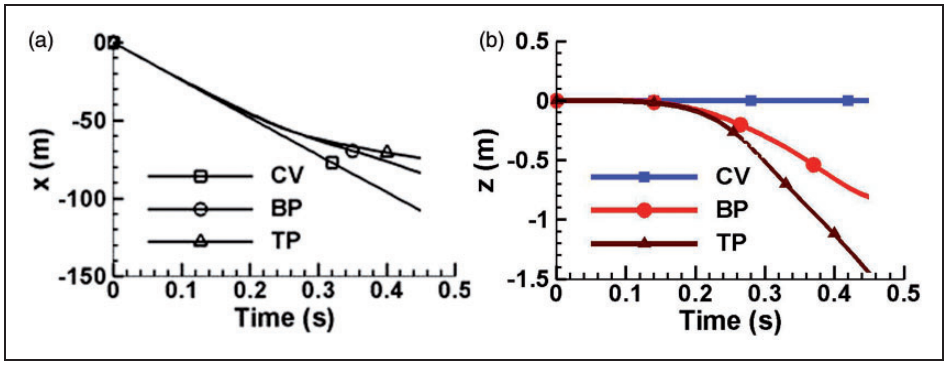

Figure 7. Time history of (a) axial displacement (m) and (b) vertical displacement (m) of CV and both the panels for Mach 0.7 with aerodynamic damping.

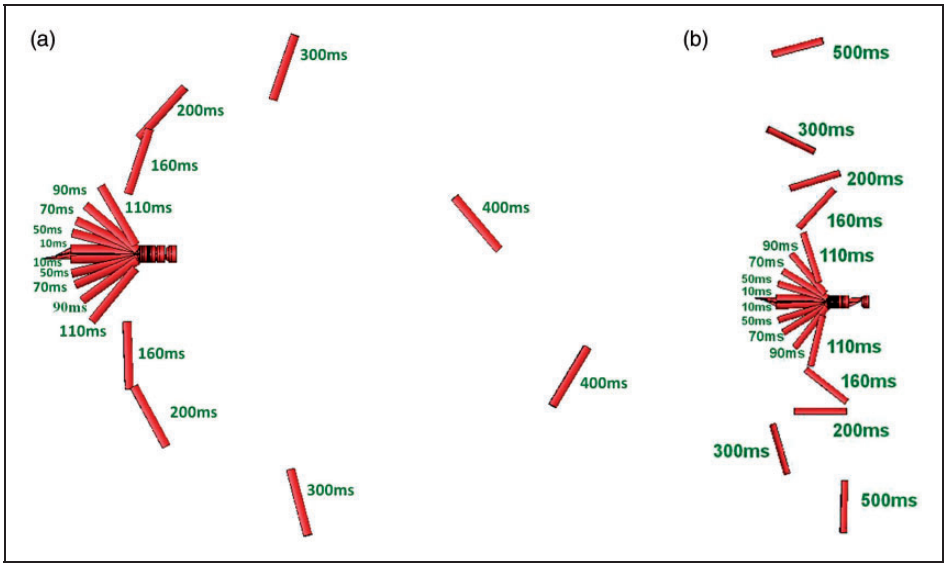

Figure 8. Panel trajectory comparisons (a) with damping and (b) without damping for Mach 0.7.

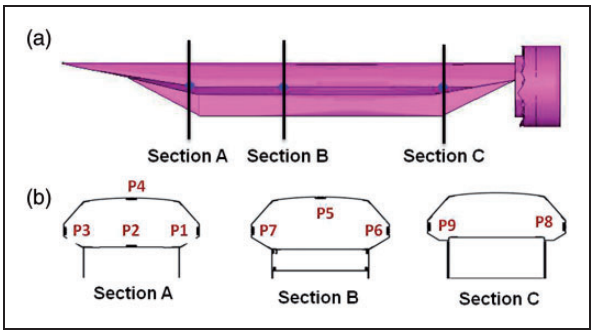

Figure 9. Pressure probe locations. (a) Axial locations and (b) azimuthal locations.

Table 2. Comparison of pressure distribution.

Probe No.	CFD	Test	% diff
p1	1.0983	1.048	4.8
p2	1.2079	1.2305	−1.8
p3	1.098	1.078	1.9
p4	1.1344	1.108	2.4
p5	1.1924	1.1755	1.4
p6	1.1867	1.198	−0.9
p7	1.1872	1.1914	−0.4
p8	1.1934	1.2124	−1.6
p9	1.1936	1.195	−0.1

are comparatively higher at lower Mach number due to dominant inertial force than aerodynamic force.

Figure 7 presents the time history of axial and vertical displacement of CV and both panels at Mach 0.7 with aerodynamic damping. The TP decelerates faster due to earlier release from the CV and reaches ground 100 ms earlier with higher downward velocity. The trajectories of panels and CV at different time instants for Mach 0.7 with and without aerodynamic damping are shown in Figures 8(a) and (b) which show safe separation. The panels are dragged behind the CV due to aerodynamic damping, where as the panels move away from CV without aerodynamic damping. Nine pressure probes were attached to CV at three axial locations as shown in Figure 9. Table 2 shows

the comparison of CFD predicted wall pressure with test when the panels are in closed condition and a good match (within 4.8% accuracy) is obtained.

Conclusions

The separation of cylindrical panels of a hypersonic air-breathing vehicle is simulated numerically for the ground test conditions. The simulations are carried out using an in-house developed separation dynamics suite consisting of pre-processor, grid free Euler solver and 6-DOF trajectory code. Simulations are carried out at Mach numbers 0.6 and 0.7 to simulate equivalent dynamic pressure and hence the order of aerodynamic forces and moments similar to that of the flight value. The predicted surface pressures at different locations compare well (within 5%) with the measured values. Without aerodynamic damping, the panels continuously traverse away from CV; whereas, with aerodynamic damping, the panels initially traverse away from the CV, later it comes back towards the CV. The trajectories of both the panels remain similar at both the Mach numbers considered. The prediction of safe separation of panels from the simulations gave confidence to the designer to go ahead with the test and computed trajectory parameters of the panels were used for test planning and placement of high speed cameras to visualize the separating panels.

Declaration of Conflicting Interests

The author(s) declared no potential conflicts of interest with respect to the research, authorship, and/or publication of this article.

Funding

The author(s) received no financial support for the research, authorship, and/or publication of this article.

References

1. Waltrup PJ. Liquid-fueled supersonic combustion ramjet: a research perspective. *J Propul Power* 1987; 3: 515–524.
2. Pannerselvam S, Thiagarajan V, Ganesh Anavardham TK, et al. Airframe integrated scramjet design and performance analysis. ISABE paper 2005-1280, 2005.
3. Dagan Y and Arad E. Analysis of shroud release applied for high-velocity missiles. *J Spacecraft Rockets* 2014; 51: 57–65.
4. Cavallo PA and Dash SM. Aerodynamics of multi-body separation using adaptive unstructured grids. In: *18th AIAA applied aerodynamics conference*, Denver, CO, 14–17 August 2000, paper no. AIAA 2000-4407.
5. Chamberlain RR. Time-accurate calculation of the HEDI shroud separation event. In: *AIAA SDIO annual interceptor technology conference*, Huntsville, AL, 19–21 May 1992, paper no. AIAA 92-2775.
6. Holden MS, Harvey J, MacLean M, et al. Development and application of a new ground test capability to conduct full-scale shroud and stage separation studies at duplicated flight conditions. In: *43rd AIAA aerospace science meeting and exhibit*, Reno, NV, 10–13 January 2005, paper no. AIAA 2005-696.
7. Raj A, Mahato M, Anandhanarayanan K, et al. ''Fairing separation studies for hypersonic technology demonstrator vehicle. In: *Proceedings of the 16th annual CFD symposium*, Bangalore, 11–12 August 2014, paper no. CP-01.
8. Szmerekovsky AG and Palazotto AN. Structural dynamic considerations for a hydrocode analysis of hypervelocity test sled impacts. *AIAA J* 2006; 44: 1350–1359.
9. Gurol H, Ketchen D, Holland L, et al. Status of the Holloman high speed MagLev test track (HHSMTT). In: *30th AIAA aerodynamic measurement technology and ground testing conference*, Atlanta, GA, 16–20 June 2014, paper no. 2014-2655.
10. Nakata D, Yajima J, Nishine K, et al. Research and development of high speed test track facility in Japan. In: *50th AIAA aerospace sciences meeting including the New Horizons forum and aerospace exposition*, Nashville, TN, 9–12 January 2012, paper no. AIAA 2012-0928.
11. Anandhanarayanan K. Development of three-dimensional grid-free solver and its applications to multi-body aerospace vehicles. *Defence Sci J* 2010; 60: 653–662.
12. Deshpande SM, Anandhanarayanan K, Praveen C, et al. Theory and applications of 3-D LSKUM based on entropy variables. *Int J Numer Meth Fluids* 2002; 40: 47–62.
13. Anandhanarayanan K, Nagarathinam M and Deshpande SM. Development and applications of a grid-free kinetic upwind solver to multi-body configurations. AIAA paper 2005-4846, June 2005.
14. Ghosh AK and Deshpande SM. Least squares kinetic upwind method for inviscid compressible flows. AIAA paper no. 95-1735, 1995.
15. Deshpande SM. Meshless method, accuracy symmetry breaking, upwinding and LSKUM. *Fluid Mechanics Report No.2003 FM 1*, Department of Aerospace Engineering, IISc, Bangalore.
16. Stokes S, Chappell JA and Leatham M. Efficient numerical store trajectory prediction for complex aircraft/store configurations. AIAA paper no. 99-3712, June 1999.
17. Anandhanarayanan K, Arora K, Shah V, et al. Separation dynamics of air-to-air-missile using a grid-free Euler solver. *AIAA J Aircraft* 2013; 50: 725–731.